

Experimental quantum natural gradient optimization in photonics

YIZHI WANG¹, SHICHUAN XUE¹, YAXUAN WANG¹, JIANGFANG DING¹, WEIXU SHI¹, DONGYANG WANG¹, YONG LIU¹, YINGWEN LIU¹, XIANG FU¹, GUANGYAO HUANG¹, ANQI HUANG¹, MINGTANG DENG¹, AND JUNJIE WU^{1,*}

¹Institute for Quantum Information & State Key Laboratory of High Performance Computing, College of Computer Science and Technology, National University of Defense Technology, Changsha 410073, China

*junjiewu@nudt.edu.cn

Compiled October 12, 2023

Variational quantum algorithms (VQAs) combining the advantages of parameterized quantum circuits and classical optimizers, promise practical quantum applications in the Noisy Intermediate-Scale Quantum era. The performance of VQAs heavily depends on the optimization method. Compared with gradient-free and ordinary gradient descent methods, the quantum natural gradient (QNG), which mirrors the geometric structure of the parameter space, can achieve faster convergence and avoid local minima more easily, thereby reducing the cost of circuit executions. We utilized a fully programmable photonic chip to experimentally estimate the QNG in photonics for the first time. We obtained the dissociation curve of the He-H⁺ cation and achieved chemical accuracy, verifying the outperformance of QNG optimization on a photonic device. Our work opens up a vista of utilizing QNG in photonics to implement practical near-term quantum applications.

© 2023 Optica Publishing Group. Users may use, reuse, and build upon the article, or use the article for text or data mining, so long as such uses are for non-commercial purposes and appropriate attribution is maintained. All other rights are reserved.

<http://dx.doi.org/10.1364/OL.494560>

Introduction.— Recently, a variety of variational quantum algorithms (VQAs) [1] have been proposed with promising applications in quantum chemistry [2, 3], materials science [4], quantum machine learning [5], and quantum information processing [6, 7], etc. VQAs employ a hybrid quantum-classical framework consisting of three building blocks: (i) preparation of parameterized quantum trial state (ansatz), (ii) estimation of the cost function, and (iii) optimization of quantum circuit parameters utilizing classical optimizers. Such a framework alleviates the heavy requirement on deep quantum circuits by leveraging additional classical resources, which promises a leading candidate to bring quantum computing to fruition in practical applications in the Noisy Intermediate-Scale Quantum (NISQ) era [8].

Significant experimental progress has been made in VQA. In photonics, there have been experimental demonstrations ranging from the first variational quantum eigensolver (VQE) [9] to combined VQEs

with phase estimation [10] and error mitigation protocols [11]. However, challenges still remain in classical optimization when scaling up: the optimization can take an extensive number of iterations, yielding a long time and high computational costs until convergence [12]. Prior experimental implementations of VQA in photonics utilized gradient-free optimizers. It is known that the gradient information of the cost function can help to guarantee and speed up the convergence of VQAs [1]. Traditional vanilla gradient descent methods have improved the VQA performance on various physical platforms, such as superconducting qubits [13, 14] and trapped ions [15, 16]. These methods assume the parameter space to be flat Euclidean, where the steepest descending direction is the negative gradient direction. Physically, however, the parameter distribution is in a Riemannian manifold, and the parametrization is not unique. Different parametrizations vary at a different rate with respect to each parameter, thus distorting distances within the optimization landscape [17, 18]. Hence, the distance should be characterized by the KL-divergence rather than Euclidean distance. Quantum natural gradient (QNG) [19] is such a quantity that uses quantum geometric information with the quantum Fisher information matrix (QFIM), which considers the distance between parameter distributions. QNG optimization moves in the steepest descent direction with respect to the quantum information geometry, corresponding to the real part of the quantum geometric tensor, known as the Fubini-Study metric. QNG has emerged as a superior optimization technique for achieving faster convergence and avoiding local minima [20].

Using a photonic chip, we experimentally demonstrate an VQE assisted by the QNG-based optimization in photonics for the first time. The chip has the full ability to (i) prepare an arbitrary quantum quart (ququart) state, (ii) perform an arbitrary projective measurement, and (iii) estimate the overlap between ququarts. We compare the convergence performance of vanilla-gradient-based VQE and QNG-based VQE in finding the ground state of the He-H⁺ cation. The QNG-based VQE shows superior convergence speed over vanilla gradient descent, achieving more than half of the reduction in optimization iterations. We employ the Simultaneous Perturbation Stochastic Approximated QNG in VQE to obtain the bond dissociation of the He-H⁺ cation, and the experimental results are all within chemical accuracy. Our experimental demonstration of QNG-based VQA applications shows that photonic platforms, especially integrated photonics, are competent in making the utmost use of gradient information in the Euclidean and Riemannian manifold space, which could lead to the acceleration of

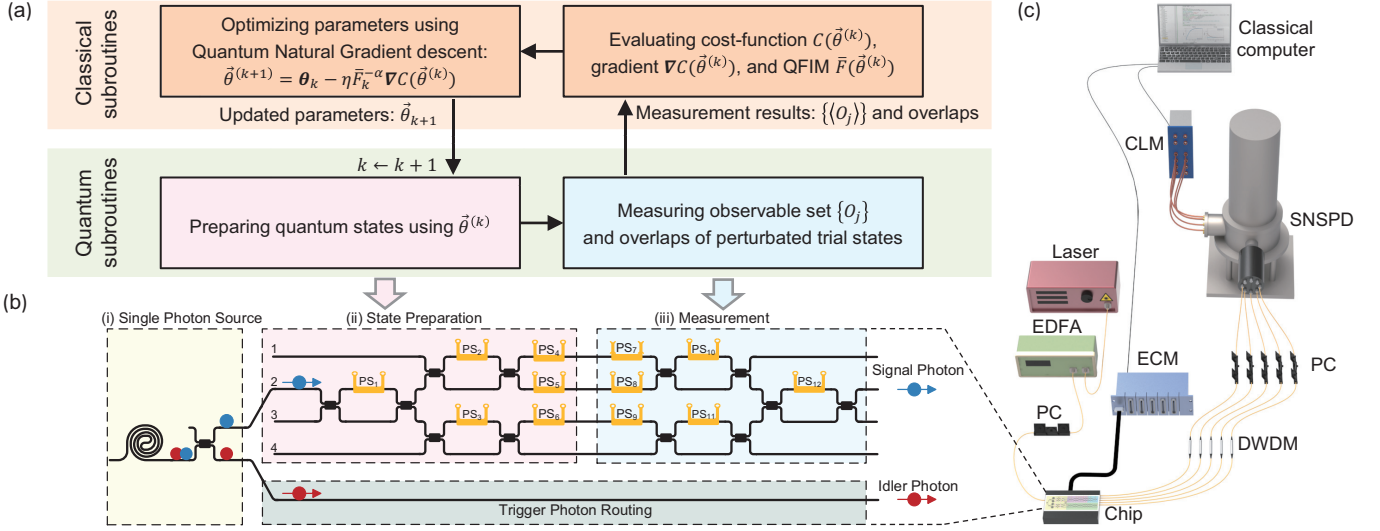


Fig. 1. Quantum natural gradient based variational quantum eigensolver and experimental setup. (A) The hybrid quantum-classical workflow of the quantum natural gradient based variational quantum eigensolver. The quantum subroutines employ the chip shown in (B), which mainly includes three functional parts: (i) the heralded single-photon source, (ii) preparing arbitrary parameterized ququart states, and (iii) performing arbitrary projective measurements. (C) Schematic of the chip with the peripheral setup. A tunable continuous wave laser is tuned to a wavelength of 1549.32 nm. The laser is amplified with an optical erbium-doped fiber amplifier (EDFA). The pump laser is launched into the packaged chip through a V-groove fiber array (VGA). Photon pairs generated from the chip are collected from the previous VGA. The signal (1554.13 nm, in blue) and idler (1544.53 nm, in red) photons are separated by dense wavelength-division multiplexing (DWDM) modules. Then photons are detected by superconducting nanowire single photon detectors (SNSPDs), and two-photon coincidence events are recorded by a coincidence logic module (CLM). The polarizations of input and output are tuned by polarization controllers (PCs). An electrical control module (ECM) configures all the on-chip thermo-optic phase shifters. A classical computer compiles optimization algorithms and coordinates control and measurement modules.

building photonic devices for practical VQA applications.

Theory of QNG-based VQE.— The VQE was first put forward to find the ground state $|\psi_G\rangle$ and ground energy E_G of the Hamiltonian for a given quantum system [9]. The Hamiltonian is typically given in the form of $H = \sum_j w_j O_j$, which is a weighted sum of Hermitian operators. The Hermitian operators O_j can be measured on the quantum hardware, and their coefficients w_j are stored in classical subroutines. VQE uses the Rayleigh-Ritz variational principle [21, 22]

$$E_G \leq \langle \psi(\vec{\theta}) | H | \psi(\vec{\theta}) \rangle \quad (1)$$

in a hybrid quantum-classical framework, involving iteratively preparing the parameterized quantum state $|\psi(\vec{\theta})\rangle$, estimating the cost function $C(\vec{\theta}) = \langle \psi(\vec{\theta}) | H | \psi(\vec{\theta}) \rangle$, and optimizing parameters $\vec{\theta}$ on the classical computer to minimize the cost function. Regarding classical optimization, we mainly considered two types of methods that use gradient information: the vanilla gradient method and the natural gradient method. The vanilla gradient method finds a local minimum of $C(\vec{\theta})$ by moving in the negative gradient direction

$$\vec{\theta}^{(k+1)} = \vec{\theta}^{(k)} - \eta \nabla C(\vec{\theta}^{(k)}), \quad (2)$$

where η is the learning rate and $\nabla C(\vec{\theta}) \in \mathbb{R}$ denotes the gradient of $C(\vec{\theta})$ with respect to all its parameters. The parameter vector $\vec{\theta}$ is updated iteratively until convergence. Nevertheless, such a naive gradient only guarantees the optimal iteration direction under a limited view of the overall cost function landscape. Hence, in physical applications, it tends to fall into local minima. The natural gradient method is motivated from the perspective of information geometry. It works well for many applications as an alternative to vanilla gradient descent. Mathematically, the natural gradient strategy follows

$$\vec{\theta}^{(k+1)} = \vec{\theta}^{(k)} - \eta F(\vec{\theta}^{(k)})^{-1} \nabla C(\vec{\theta}^{(k)}), \quad (3)$$

where $F(\vec{\theta})$ is the quantum Fisher information matrix (QFIM) with the element as $F_{ij}(\vec{\theta}) = \text{Re} \left\{ \left\langle \frac{\partial \psi}{\partial \theta_i} \middle| \frac{\partial \psi}{\partial \theta_j} \right\rangle - \left\langle \frac{\partial \psi}{\partial \theta_i} \middle| \psi(\vec{\theta}) \right\rangle \left\langle \psi(\vec{\theta}) \middle| \frac{\partial \psi}{\partial \theta_j} \right\rangle \right\}$.

However, obtaining each of the QFIM elements requires expensive computational costs [18, 20]. Alternatively, the QFIM can be estimated with the Simultaneous Perturbation Stochastic Approximation (SPSA) algorithm [23]. Instead of computing all elements in each iteration, we can sample the QFIM using two random directions Δ_1 and Δ_2 . Given the Fisher information metric in the state overlap form as

$$f(\vec{\theta}_1, \vec{\theta}_2) = \left| \langle \psi(\vec{\theta}_1) | \psi(\vec{\theta}_2) \rangle \right|^2, \quad (4)$$

the estimated QFIM $\tilde{F}(\vec{\theta}^{(k)})$ can be obtained by $\tilde{F}(\vec{\theta}^{(k)}) = \frac{\delta F(\vec{\theta}^{(k)})}{2\epsilon^2} \frac{\Delta_1 \Delta_1^T + \Delta_2 \Delta_2^T}{2}$, where ϵ is the perturbation rate, and

$$\delta F(\vec{\theta}^{(k)}) = f(\vec{\theta}^{(k)}, \vec{\theta}^{(k)} + \epsilon \Delta_1 + \epsilon \Delta_2) - f(\vec{\theta}^{(k)}, \vec{\theta}^{(k)} + \epsilon \Delta_1) - f(\vec{\theta}^{(k)}, \vec{\theta}^{(k)} - \epsilon \Delta_1 + \epsilon \Delta_2) + f(\vec{\theta}^{(k)}, \vec{\theta}^{(k)} - \epsilon \Delta_1). \quad (5)$$

The point sample $\tilde{F}(\vec{\theta}^{(k)})$ is then combined with all the previous samples in an exponentially smoothed estimator $\bar{F}^{(k)} = \frac{k}{k+1} \bar{F}^{(k-1)} + \frac{1}{k+1} \tilde{F}(\vec{\theta}^{(k)})$. Then the SPSA-QNG descent update rule is given by

$$\vec{\theta}^{(k+1)} = \vec{\theta}^{(k)} - \eta (\bar{F}^{(k)})^{-\alpha} \nabla C(\vec{\theta}^{(k)}). \quad (6)$$

Here, α is considered a regularization parameter to avoid unstable update caused by possibly ill-conditioned $\bar{F}(\vec{\theta}^{(k)})$ [24]. In our experiments, we set $\alpha = 0.5$ for a stable half-inversion.

As shown in Fig. 1(A), the QNG-based VQE is mainly composed of the following steps [1, 9, 25]:

(i) (*Quantum subroutine*) Prepare trial states $|\psi(\vec{\theta})\rangle$ using a parameterized circuit $U(\vec{\theta})$.

(ii) (*Quantum subroutine*) Estimate groups of observables $\{O_j\}$ that constitute the Hamiltonian H , and overlaps of trial states with perturbed parameters as shown in $\delta F(\vec{\theta}^{(k)})$.

(iii) (*Classical subroutine*) Evaluate the cost function $C(\vec{\theta})$ and its gradient $\nabla C(\vec{\theta}^{(k)})$ from the set of measurement results $\{\langle O_j \rangle\}$, and evaluate the QFIM $\hat{F}(\vec{\theta}^{(k)})$ from the overlaps of perturbed trial states.

(iv) (*Classical subroutine*) Based on the SPSA-QNG descent update rule in Eq. (6), update the parameters $\vec{\theta}$ to minimize the expectation value.

(v) Repeat steps (i)-(iv) until the desired accuracy is reached.

Experimental methods.— We experimentally demonstrate the QNG-based VQE to estimate the ground state energy of the He-H⁺ cation [9, 11] in a four-dimensional Hilbert space, using parts of a reconfigurable silicon photonic chip [26] that can high precisely (i) prepare arbitrary ququart states, (ii) estimate the overlap between ququarts, and (iii) perform an arbitrary projective measurement. The Pauli operators and coefficients constituting the He-H⁺ Hamiltonian with respect to different interatomic distances are listed in Table S1 of Supplement 1. The schematic of the chip and the external setup is shown in Fig. 1. We mainly use three functional parts of the chip. In the single-photon source part, a spiral-waveguide spontaneous four-wave mixing (SFWM) photon-pair source [27] is pumped. The post-selected signal and idler photons are sent to the state preparing part and passed directly to the detectors, respectively. One idler photon is detected to herald a single signal photon sent to the following operations. The average coincidence rate is ~ 4.5 kHz.

With the state preparation circuit consisting of three programmable Mach-Zehnder interferometers and three external phase shifters, an arbitrary trial ququart state $|\psi(\vec{\theta})\rangle$ can be generated using the four-dimensional path mode of the heralded photon [28]. Together with the following measurement part, the overlap

$$D(|\psi(\vec{\theta}_1)\rangle, |\psi(\vec{\theta}_2)\rangle) = \left| \langle \psi(\vec{\theta}_1) | \psi(\vec{\theta}_2) \rangle \right|^2 \quad (7)$$

between two parameterized ququarts $|\psi(\vec{\theta}_1)\rangle$ and $|\psi(\vec{\theta}_2)\rangle$ can be estimated. The configuration methods for the on-chip phase shifters (PS₁ \sim PS₁₂) to prepare the trial state $|\psi(\vec{\theta})\rangle$ and estimate the ququart overlap $D(|\psi(\vec{\theta}_1)\rangle, |\psi(\vec{\theta}_2)\rangle)$ are detailed in Section 1 of Supplement 1.

We are able to further estimate the result of arbitrary projective measurement. Given a projective measurement described by a Hermitian operator O and the observable has a spectral decomposition $O = \sum_j m_j P_j$. Here $P_j = |m_j\rangle \langle m_j|$ is the projector onto the j -th eigenspace of O with eigenvalue m_j and corresponding normalized eigenvector $|m_j\rangle$ [29]. We can estimate the overlap between $|\psi(\vec{\theta})\rangle$ and each eigenspace $D(|\psi(\vec{\theta})\rangle, |m_j\rangle)$. Then the average value of the measurement of O upon $|\psi(\vec{\theta})\rangle$ can be obtained by

$$E(O) = \langle \psi(\vec{\theta}) | O | \psi(\vec{\theta}) \rangle = \sum_j m_j D(|\psi(\vec{\theta})\rangle, |m_j\rangle). \quad (8)$$

Accordingly, given the Hamiltonian in the form of $H = \sum_j w_j O_j$, the cost function value $C(\vec{\theta})$ can be obtained by weighted summing all the $E(O_j)$.

The full abilities of the chip for quantum information processing allow us to extract the analytical gradient in Euclidean space and QFIM from the information geometry. The partial derivative of the cost function $C(\vec{\theta})$ with respect to the photonics phase shift $\theta^{(k)}$ can be estimated using the hardware-friendly parameter-shift rule [30]

$$\frac{\partial C(\vec{\theta})}{\partial \theta_j} = \frac{C(\vec{\theta}_{j+}) - C(\vec{\theta}_{j-})}{\sqrt{2}}, \quad (9)$$

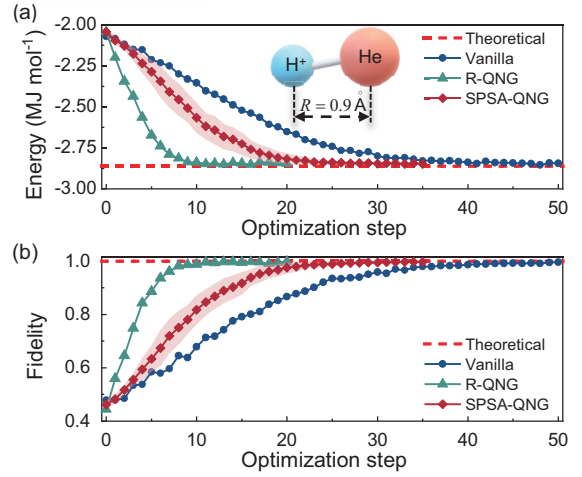


Fig. 2. Finding the ground state of the He-H⁺ cation at the interatomic distance of $R = 0.9$ Å. A comparison of the convergence performance of the evolution of (A) energy and (B) fidelity using vanilla gradient descent (Vanilla), rigorous quantum natural gradient descent (R-QNG), and Simultaneous Perturbation Stochastic Approximated quantum natural gradient descent (SPSA-QNG). For SPSA-QNG, we repeat the optimization ten times and plot the average and standard deviation (shaded area) of the energy and fidelity in these ten optimizations.

with $\vec{\theta}_{j\pm} = \vec{\theta} \pm \frac{\pi}{4} \mathbf{e}_j$. Here, \mathbf{e}_j is a unit vector with 1 as its j -th element and 0 otherwise. Thus, we estimate the analytical gradient $\frac{\partial C(\vec{\theta})}{\partial \theta_j}$ with two additional measurements that only change the original phase shift θ_j to $\theta_j + \frac{\pi}{4}$ and $\theta_j - \frac{\pi}{4}$, respectively. Reviewing Eq. (6), we can approximate the QFIM by obtaining the Fisher information metrics from the four overlaps of states with different perturbations.

Experimental results.— Before running the variational application, we first characterize the high-precision of our chip with one thousand quantum state preparation and measurement experiments. In each experiment, we program the preparation part of the chip to generate the target random ququart state $|\psi_{\text{the}}\rangle$, and the measurement part to estimate the overlap between the generated ququart $|\psi_{\text{exp}}\rangle$ and $|\psi_{\text{the}}\rangle$. After collecting the heralded photons from the four output ports, the overlap $D(|\psi_{\text{the}}\rangle, |\psi_{\text{exp}}\rangle)$ can be obtained from the probability of heralded photons at the second port. The statistical quantum state fidelity $F = \sqrt{D(|\psi_{\text{the}}\rangle, |\psi_{\text{exp}}\rangle)}$ [29] reaches as high as $99.77 \pm 0.11\%$. The histogram of measured fidelities is shown in Fig. S1 of Supplement 1.

By harnessing our photonic chip to obtain gradient and QNG, we experimentally compare the convergence performance of VQE with three types of gradient-based optimizers, using the Hamiltonian for He-H⁺ at the interatomic distance $R = 0.9$ Å and an initial trial superposition state $|\psi_0\rangle = [0.5, 0.5, 0.5, 0.5]^T$. As illustrated in Fig. 2 and Table S2, we present the convergence of the trial state energy and fidelity with the theoretical ground state using a learning rate of $\eta = 0.05\pi$ and a perturbation of $\epsilon = 0.05\pi$. The advantage of QNG is clearly its superior convergence speed compared to vanilla gradient descent. It achieves more than half of the reduction in optimization steps until the energy fluctuation is less than 10^{-2} MJ mol⁻¹. For SPSA-QNG, even though the convergence speed is slightly worse than rigorous QNG, it almost halves the optimization iterations over vanilla gradient descent. The average fidelity of the obtained ground states reaches $99.64 \pm 0.21\%$.

To obtain the bond dissociation energy of the He-H⁺ cation, we use the SPSA-QNG-based VQE to search for ground states at a range of

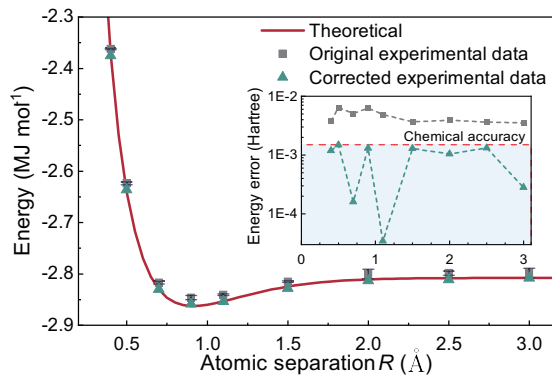


Fig. 3. Dissociation curve of the He–H⁺ cation. For the SPSA-QNG data, the energy and its error bar are obtained by averaging and calculating the standard deviation of results from ten repeated SPSA-QNG VQE runs. In each run, the final energy is obtained by averaging the measured energy values over five steps after convergence. After correcting for a constant systematic error, the data overlaps well with the theoretical energy curve, and the absolute errors (shown in the inset) achieve chemical accuracy.

nuclear separations R . In Fig. 3, the experimental results show good agreement with the theoretical ground-state energies. The experimental data is obtained from the average of ten optimizations at each interatomic distance. After correction for a constant shift $\varepsilon_c = 0.013 \text{ MJ mol}^{-1}$ [9], all absolute errors are less than $3.938 \text{ KJ mol}^{-1}$ (0.0015 Hartree), achieving chemical accuracy. For more details, see Section 2, Table S3, and Fig. S2 of Supplement 1.

Conclusion.— Compared with general gradient-based optimization methods that omit the geometry of the parameter space, quantum natural gradient optimization methods utilize quantum geometric information and adjust the gradient direction accordingly. This approach provides faster convergence and improved robustness, which has been verified in various VQA applications through numerical simulation [19, 23, 24].

We used a silicon photonic chip to implement VQEs that are equipped with QNG. We experimentally obtained the ground energies of the He–H⁺ cation at a series of interatomic distances and achieved chemical accuracy. From this, we showed that QNG-based optimization has a superior convergence speed over vanilla gradient descent, achieving almost half of the reduction in optimization iterations. Our work has demonstrated the feasibility and superiority of the QNG-based optimization method in photonics. It has shed light on implementing practical quantum applications in the NISQ era.

Funding. National Natural Science Foundation of China (62061136011, 62105366, and 62075243).

Disclosures. The authors declare no conflicts of interest.

Data availability. Data underlying the results presented in this paper are not publicly available at this time but may be obtained from the authors upon reasonable request.

Supplemental document. See Supplement 1 for supporting content.

REFERENCES

- M. Cerezo, A. Arrasmith, R. Babbush, S. C. Benjamin, S. Endo, K. Fujii, J. R. McClean, K. Mitarai, X. Yuan, L. Cincio, and P. J. Coles, *Nat. Rev. Phys.* **3**, 625 (2021).
- S. McArdle, S. Endo, A. Aspuru-Guzik, S. C. Benjamin, and X. Yuan, *Rev. Mod. Phys.* **92**, 015003 (2020).
- Y. Li, J. Hu, X. Zhang, Z. Song, and M. Yung, *Adv. Theory Simulations* **2**, 1800182 (2019).
- B. Bauer, S. Bravyi, M. Motta, and G. K.-L. Chan, *Chem. Rev.* **120**, 12685 (2020).
- S.-X. Zhang, Z.-Q. Wan, C.-K. Lee, C.-Y. Hsieh, S. Zhang, and H. Yao, *Phys. Rev. Lett.* **128**, 120502 (2022).
- Y. Liu, D. Wang, S. Xue, A. Huang, X. Fu, X. Qiang, P. Xu, H.-L. Huang, M. Deng, C. Guo, X. Yang, and J. Wu, *Phys. Rev. A* **101**, 052316 (2020).
- S. Xue, Y. Liu, Y. Wang, P. Zhu, C. Guo, and J. Wu, *Phys. Rev. A* **105**, 032427 (2022).
- J. Preskill, *Quantum* **2**, 79 (2018).
- A. Peruzzo, J. McClean, P. Shadbolt, M.-H. Yung, X.-Q. Zhou, P. J. Love, A. Aspuru-Guzik, and J. L. O’Brien, *Nat. Commun.* **5**, 4213 (2014).
- R. Santagati, J. Wang, A. A. Gentile, S. Paesani, N. Wiebe, J. R. McClean, S. Morley-Short, P. J. Shadbolt, D. Bonneau, J. W. Silverstone, D. P. Tew, X. Zhou, J. L. O’Brien, and M. G. Thompson, *Sci. Adv.* **4**, eaap9646 (2018).
- D. Lee, J. Lee, S. Hong, H.-T. Lim, Y.-W. Cho, S.-W. Han, H. Shin, J. Ur Rehman, and Y.-S. Kim, *Optica* **9**, 88 (2022).
- L. Bittel and M. Kliesch, *Phys. Rev. Lett.* **127**, 120502 (2021).
- A. Kandala, A. Mezzacapo, K. Temme, M. Takita, M. Brink, J. M. Chow, and J. M. Gambetta, *Nature* **549**, 242 (2017).
- Google AI Quantum and Collaborators, *Science* **369**, 1084 (2020).
- C. Hempel, C. Maier, J. Romero, J. McClean, T. Monz, H. Shen, P. Jurcevic, B. P. Lanyon, P. Love, R. Babbush, A. Aspuru-Guzik, R. Blatt, and C. F. Roos, *Phys. Rev. X* **8**, 031022 (2018).
- L. Zhao, J. Goings, K. Wright, J. Nguyen, J. Kim, S. Johri, K. Shin, W. Kyoung, J. I. Fuks, J.-K. K. Rhee, and Y. M. Rhee, *arXiv:2212.02482* (2022).
- S.-i. Amari, *Neural Comput.* **10**, 251 (1998).
- N. Yamamoto, *arXiv:1909.05074* (2019).
- J. Stokes, J. Izaac, N. Killoran, and G. Carleo, *Quantum* **4**, 269 (2020).
- D. Wierichs, C. Gogolin, and M. Kastoryano, *Phys. Rev. Res.* **2**, 043246 (2020).
- J. W. Rayleigh, *Phil. Trans.* **161**, 77 (1870).
- W. Ritz, *J. Reine Angew. Math.* **135**, 1 (1908).
- J. Gacon, C. Zoufal, G. Carleo, and S. Woerner, *Quantum* **5**, 567 (2021).
- T. Haug and M. S. Kim, *arXiv:1909.05074* (2021).
- J. Tilly, H. Chen, S. Cao, D. Picozzi, K. Setia, Y. Li, E. Grant, L. Wossnig, I. Rungger, G. H. Booth, and J. Tennyson, *Phys. Reports* **986**, 1 (2022).
- S. Xue, Y. Wang, J. Zhan, Y. Wang, R. Zeng, J. Ding, W. Shi, Y. Liu, Y. Liu, A. Huang, G. Huang, C. Yu, D. Wang, X. Fu, X. Qiang, P. Xu, M. Deng, X. Yang, and J. Wu, *Phys. Rev. Lett.* **129**, 133601 (2022).
- J. W. Silverstone, D. Bonneau, K. Ohira, N. Suzuki, H. Yoshida, N. Iizuka, M. Ezaki, C. M. Natarajan, M. G. Tanner, R. H. Hadfield, V. Zwiller, G. D. Marshall, J. G. Rarity, J. L. O’Brien, and M. G. Thompson, *Nat. Photonics* **8**, 104 (2014).
- M. Reck, A. Zeilinger, H. J. Bernstein, and P. Bertani, *Phys. Rev. Lett.* **73**, 58 (1994).
- M. A. Nielsen and I. L. Chuang, *Quantum Computation and Quantum Information* (Cambridge University Press, Cambridge ; New York, 2010), 10th ed.
- A. Mari, T. R. Bromley, and N. Killoran, *Phys. Rev. A* **103**, 012405 (2021).

Experimental quantum natural gradient optimization in photonics: supplemental document

1. SUPPLEMENTARY METHOD: ON-CHIP PREPARATION OF ARBITRARY QUQUART STATES AND ESTIMATION OF OVERLAP BETWEEN QUQUARTS

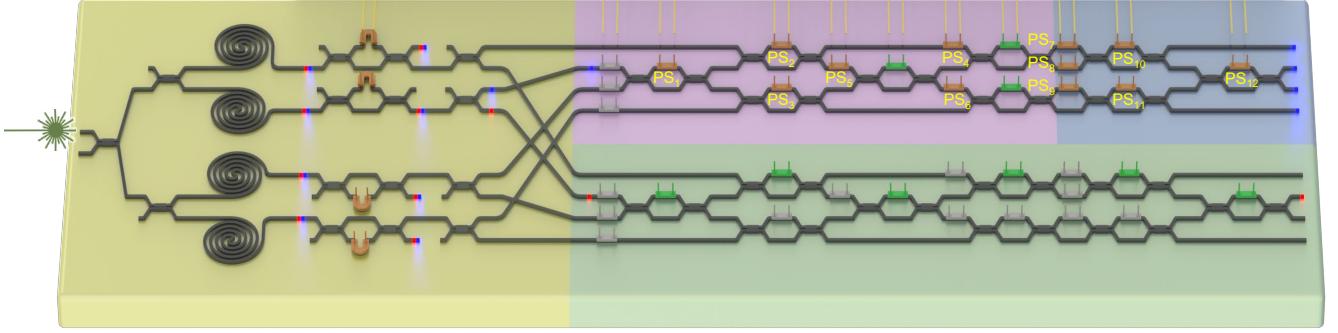


Fig. S1. Schematic of the reconfigurable silicon photonic chip used in the experimental quantum natural gradient optimization. The chip monolithically embeds 4 spontaneous four-wave mixing photon-pair sources, 40 reconfigurable thermo-optic phase shifters, and 44 multimode interferometers. In our experiments, the phase shifters colored in gray stay as spares. We set the phase shifters colored in green as π . The 12 phase shifters colored in brown are labeled as $PS_1 \sim PS_{12}$ in the main text Fig. 1, which are used to prepare ququart states and perform projective measurement.

We use parts of a reconfigurable silicon photonic chip [1] to perform experimental demonstrations. In the heralded single-photon source part, four spiral-waveguide spontaneous four-wave mixing photon-pair sources [2] are coherently pumped. By configuring the four asymmetric Mach-Zehnder interferometers [3], the photon pairs from the second source are retained while that from the other three sources are filtered out of the chip. The post-selected signal and idler photons are sent to the ququart state preparation part and passed through the trigger routing part to the detectors, respectively.

In the state preparation part, we can prepare an arbitrary ququart state using the heralded photon. Note that any ququart state can be decomposed into the parametric form [4]:

$$\begin{aligned} |\psi(\vec{\theta})\rangle &= |\psi(\theta_1, \theta_2, \theta_3, \phi_1, \phi_2, \phi_3, \phi_4)\rangle \\ &= e^{i\phi_1} \sin \theta_1 \sin \theta_2 |1\rangle + e^{i\phi_2} \sin \theta_1 \cos \theta_2 |2\rangle + e^{i\phi_3} \cos \theta_1 \sin \theta_3 |3\rangle + e^{i\phi_4} \cos \theta_1 \cos \theta_3 |4\rangle, \end{aligned} \quad (S1)$$

where $|k\rangle$ ($k=1,2,3,4$) is the path mode of the heralded photon. With the circuit consisting of three programmable Mach-Zehnder interferometers (of which the phase shifters are PS_1 , PS_2 , and PS_3) and another three extra phase shifters (PS_4 , PS_5 , and PS_6), we can generate the ququart state given in the form of Eq.(S1) as $|\psi_S(\vec{\theta}_S)\rangle = |\psi_S(\theta_{S1}, \theta_{S2}, \theta_{S3}, \phi_{S1}, \phi_{S2}, \phi_{S3}, \phi_{S4})\rangle$ by setting the phase shifters as:

$$\begin{aligned} \varphi_{PS_1} &= 2\theta_{S1}, & \varphi_{PS_4} &= \phi_{S1} - \phi_{S4} - \theta_{S2} + \theta_{S3} + \frac{\pi}{2}, \\ \varphi_{PS_2} &= \pi + 2\theta_{S2}, & \varphi_{PS_5} &= \phi_{S2} - \phi_{S4} - \theta_{S2} + \theta_{S3} + \frac{\pi}{2}, \\ \varphi_{PS_3} &= 2\theta_{S3}, & \varphi_{PS_6} &= \phi_{S3} - \phi_{S4}. \end{aligned} \quad (S2)$$

Then the ququart preparing operation on the heralded photon $U_{\text{prep}} = U_{\text{prep}}(\varphi_{PS_1}, \varphi_{PS_2}, \varphi_{PS_3}, \varphi_{PS_4}, \varphi_{PS_5}, \varphi_{PS_6})$ generates the evolved state $|\psi_{\text{prep}}\rangle = U_{\text{prep}}|2\rangle$, which is equal to $|\psi_S(\vec{\theta}_S)\rangle$ up to a global phase factor $e^{-i(\theta_{S1} + \theta_{S3} - \phi_{S4} + \pi)}$. For example, in our experiments to find ground states of the He-H^+ cation, the phase shifts for the initial trial superposition state $|\psi_0\rangle = [0.5, 0.5, 0.5, 0.5]^T$ are $\vec{\varphi}_0 = [\frac{\pi}{2}, \frac{3\pi}{2}, \frac{\pi}{2}, \frac{\pi}{2}, \frac{\pi}{2}, 0]^T$.

The overlap

$$D(|\psi_S(\vec{\theta}_S)\rangle, |\psi_M(\vec{\theta}_M)\rangle) = \left| \langle \psi_S(\vec{\theta}_S) | \psi_M(\vec{\theta}_M) \rangle \right|^2 \quad (S3)$$

between the ququarts $|\psi_S(\vec{\theta}_S)\rangle$ and $|\psi_M(\vec{\theta}_M)\rangle = |\psi_M(\theta_{M1}, \theta_{M2}, \theta_{M3}, \phi_{M1}, \phi_{M2}, \phi_{M3}, \phi_{M4})\rangle$, can be estimated by using the following measurement circuit to implement the inverse of the preparation operation of $|\psi_M(\vec{\theta}_M)\rangle$. When the phase shifts for the following six phase shifters are:

$$\begin{aligned}\varphi_{PS_7} &= -\phi_{M1} + \phi_{M4} - \theta_{M2} + \theta_{M3} + \frac{\pi}{2}, & \varphi_{PS_{10}} &= \pi + 2\theta_{M2}, \\ \varphi_{PS_8} &= -\phi_{M2} + \phi_{M4} - \theta_{M2} + \theta_{M3} + \frac{\pi}{2}, & \varphi_{PS_{11}} &= 2\theta_{M3}, \\ \varphi_{PS_9} &= -\phi_{M3} + \phi_{M4}, & \varphi_{PS_{12}} &= 2\theta_{M1},\end{aligned}\tag{S4}$$

the operation $U_{\text{proj}} = U_{\text{proj}}(\varphi_{PS_7}, \varphi_{PS_8}, \varphi_{PS_9}, \varphi_{PS_{10}}, \varphi_{PS_{11}}, \varphi_{PS_{12}})$ has the relation $U_{\text{proj}}|\psi_M(\vec{\theta}_M)\rangle = e^{i(\theta_{M1} + \theta_{M3} + \phi_{M4} + \pi)}|2\rangle$. Then the detection probability of heralded photon at the second output port is:

$$\begin{aligned}P_{(2)} &= |\langle 2|U_{\text{proj}}|\psi_{\text{prep}}\rangle|^2 \\ &= |\langle \psi_M(\vec{\theta}_M)|U_{\text{proj}}^\dagger U_{\text{proj}}|\psi_S(\vec{\theta}_S)\rangle|^2 \\ &= |\langle \psi_M(\vec{\theta}_M)|\psi_S(\vec{\theta}_S)\rangle|^2 \\ &= D(|\psi_S(\vec{\theta}_S)\rangle, |\psi_M(\vec{\theta}_M)\rangle).\end{aligned}\tag{S5}$$

Accordingly, the overlap between arbitrary ququarts can be experimentally estimated. Note that in experiments, the phase shifts for $PS_4 \sim PS_6$ should add π to offset the extra phase caused by the three "green" shifters in the state preparation part.

2. SUPPLEMENTARY METHOD: ESTIMATING THE SYSTEMATIC ERROR IN MEASURING HAMILTONIANS OF THE HE-H⁺ CATION

The existence of systematic errors is common when implementing VQEs on NISQ devices, from photonics [5] and superconducting qubits [6] to trapped ions [7]. Systematic effects, such as imperfections in the fabrication of the quantum circuit, control noise, and residual crosstalk, contribute to the shift of the measured results of the Hamiltonian. For the specific group of Hamiltonians, systematic errors often manifest as a constant shift, and correction of systematic errors requires first estimating the shift. For example, Ref. [5] observed a constant and reproducible small shift from the experimentally obtained bond dissociation curve and the theoretical curve. They shifted the experimental results by this constant. Ref. [7] shifted all the measured energies so that the energy at a specific interatomic distance matches the simulation energy. In fact, correction methods of Refs. [5] and [7] will mix two sources of error: the systematic error and the optimization (algorithm) error. This is because the VQE optimization results may converge to inaccurate ground states, and the experimentally obtained ground energies will also include the optimization error.

As shown in the inset of Fig. 3 in the main text, we observed small energy errors within the same order of magnitude in all the experimentally obtained ground energies of the He-H⁺ cation with respect to different interatomic distances. Systematic effects, such as imperfections in the fabrication of the photonic circuit, control noise of the electrical control module, and crosstalk of the phase shifters, contribute to the shift of the measured results of Pauli strings. The weighted sum of these shifted measurement values of Pauli strings leads to the systematic error of our experimental results.

To estimate the exact systematic error, we exclude the optimization error by measuring the ground energy using the calculated parameters for the exact ground state (obtained by exact diagonalization). We determine the systematic correction value by measuring the ground energy for the exact ground state of the He-H⁺ cation at $R = 0.9 \text{ \AA}$. The error between the measured value ($2.8495 \text{ MJ mol}^{-1}$) and theoretical value ($2.8626 \text{ MJ mol}^{-1}$) is $0.0131 \text{ MJ mol}^{-1}$. This measured error gives an estimation of the systematic error at different interatomic distances. After correcting for this constant correction value, our experimental data achieves chemical accuracy.

3. SUPPLEMENTARY TABLES

Table S1. The table of Pauli strings and their coefficients constituting the He-H⁺ Hamiltonian with respect to various interatomic distance R [5], of which the ground states are experimentally solved in our demonstrations.

$R(\text{\AA})$	II	IX	IZ	XI	XX	XZ	ZI	ZX	ZZ
0.4	-1.3119	-0.1396	-1.7568	-0.1396	0.3352	0.1396	-1.7568	0.1396	0.0969
0.5	-2.3275	-0.157	-1.5236	-0.157	0.3309	0.157	-1.5236	0.157	0.1115
0.7	-3.3893	-0.1968	-1.2073	-0.1968	0.3052	0.1968	-1.2073	0.1968	0.1626
0.9	-3.8505	-0.2288	-1.0466	-0.2288	0.2613	0.2288	-1.0466	0.2288	0.2356
1.1	-4.0539	-0.243	-0.982	-0.243	0.2053	0.243	-0.982	0.243	0.3225
1.5	-4.1594	-0.2086	-0.991	-0.2086	0.0948	0.2086	-0.991	0.2086	0.4945
2	-4.1347	-0.1119	-1.0605	-0.1119	0.0212	0.1119	-1.0605	0.1119	0.6342
2.5	-4.0918	-0.0454	-1.1128	-0.0454	0.0032	0.0454	-1.1128	0.0454	0.701
3	-4.0578	-0.0159	-1.1482	-0.0159	0.0004	0.0159	-1.1482	0.0159	0.7385

Table S3. Experimental results for the dissociation curve of the He-H⁺ cation shown in Fig. 3. The energy, fidelity, and their errors are obtained by the average and standard deviation of results from ten repeated SPSA-QNG runs. In each run, the final energy is obtained using the average of measured energy values over five steps after convergence. After correcting for a constant systematic error, the data agree well with the theoretical energy, and the absolute error achieves chemical accuracy (1.5E-03 Hartree).

R (Å)	Theoretical energy (MJ mol ⁻¹)	SPSA-QNG			Corrected	
		Energy (MJ mol ⁻¹)	Fidelity	Energy error (Hartree)	Energy (MJ mol ⁻¹)	Energy error (Hartree)
0.4	-2.372	-2.362±0.001	99.89 ± 0.02%	3.767E-03	-2.375	1.185E-03
0.5	-2.641	-2.624±0.003	99.77 ± 0.05%	6.433E-03	-2.637	1.482E-03
0.7	-2.831	-2.817±0.002	99.74 ± 0.06%	5.111E-03	-2.830	1.600E-04
0.9	-2.863	-2.846±0.004	99.64 ± 0.20%	6.262E-03	-2.859	1.310E-03
1.1	-2.854	-2.841±0.002	99.65 ± 0.12%	4.917E-03	-2.854	3.428E-05
1.5	-2.825	-2.815±0.001	99.70 ± 0.30%	3.656E-03	-2.828	1.295E-03
2	-2.811	-2.801±0.009	99.12 ± 1.01%	3.908E-03	-2.814	1.043E-03
2.5	-2.808	-2.799±0.004	99.74 ± 0.54%	3.627E-03	-2.812	1.324E-03
3	-2.808	-2.799±0.009	98.60 ± 1.35%	3.529E-03	-2.809	2.799E-04

4. SUPPLEMENTARY FIGURES

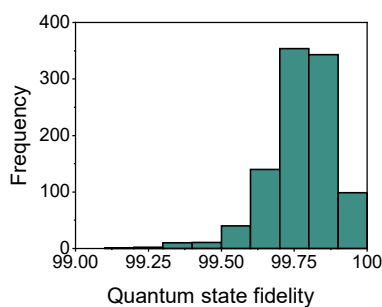


Fig. S2. Histogram of the statistic quantum state fidelities for 1,000 randomly generated quantum states in the four-dimensional Hilbert space.

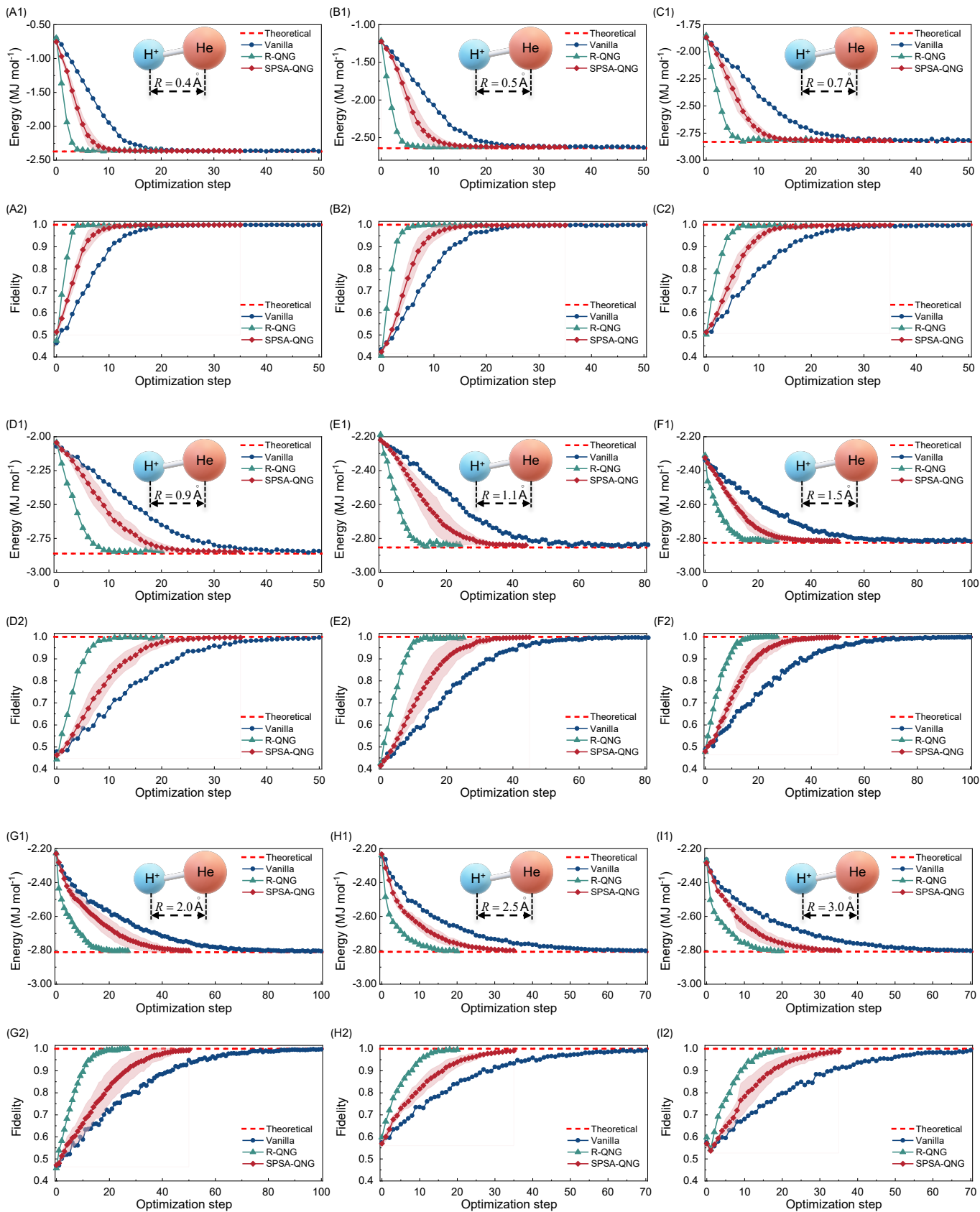


Fig. S3. Finding the ground states of He-H⁺ cation at the interatomic distance (A) $R = 0.4 \text{ \AA}$, (B) $R = 0.5 \text{ \AA}$, (C) $R = 0.7 \text{ \AA}$, (D) $R = 0.9 \text{ \AA}$, (E) $R = 1.1 \text{ \AA}$, (F) $R = 1.5 \text{ \AA}$, (G) $R = 2.0 \text{ \AA}$, (H) $R = 2.5 \text{ \AA}$, and (I) $R = 3.0 \text{ \AA}$. A comparison of the convergence performance of the evolution of energy and fidelity with vanilla gradient descent (Vanilla), rigorous quantum natural gradient descent (R-QNG), and simultaneous perturbation stochastic approximated quantum natural gradient descent (SPSA-QNG) is presented. For SPSA-QNG, we repeat the optimization ten times, and the average and standard deviation (shaded area) of the energy and fidelity in the ten optimizations are plotted.

REFERENCES

1. S. Xue, Y. Wang, J. Zhan, Y. Wang, R. Zeng, J. Ding, W. Shi, Y. Liu, Y. Liu, A. Huang, G. Huang, C. Yu, D. Wang, X. Fu, X. Qiang, P. Xu, M. Deng, X. Yang, and J. Wu, "Variational Entanglement-Assisted Quantum Process Tomography with Arbitrary Ancillary Qubits," *Phys. Rev. Lett.* **129**, 133601 (2022).
2. J. W. Silverstone, D. Bonneau, K. Ohira, N. Suzuki, H. Yoshida, N. Iizuka, M. Ezaki, C. M. Natarajan, M. G. Tanner, R. H. Hadfield, V. Zwiller, G. D. Marshall, J. G. Rarity, J. L. O'Brien, and M. G. Thompson, "On-chip quantum interference between silicon photon-pair sources," *Nat. Photonics* **8**, 104–108 (2014).
3. Y. Liu, C. Wu, X. Gu, Y. Kong, X. Yu, R. Ge, X. Cai, X. Qiang, J. Wu, X. Yang, and P. Xu, "High-spectral-purity photon generation from a dual-interferometer-coupled silicon microring," *Opt. Lett.* **45**, 73 (2020).
4. M. Reck, A. Zeilinger, H. J. Bernstein, and P. Bertani, *Phys. Rev. Lett.* **73**, 58 (1994).
5. A. Peruzzo, J. McClean, P. Shadbolt, M.-H. Yung, X.-Q. Zhou, P. J. Love, A. Aspuru-Guzik, and J. L. O'Brien, "A variational eigenvalue solver on a photonic quantum processor," *Nat. Commun.* **5**, 4213 (2014).
6. A. Kandala, K. Temme, A. D. Córcoles, A. Mezzacapo, J. M. Chow, and J. M. Gambetta, *Nature* **567**, 491 (2019).
7. L. Zhao, J. Goings, K. Wright, J. Nguyen, J. Kim, S. Johri, K. Shin, W. Kyoung, J. I. Fuks, J.-K. K. Rhee, and Y. M. Rhee, arXiv:2212.02482 (2022).